1

Chemical Processing of Mixed-Cation Hybrid Perovskites: Stabilizing Effects of Configurational Entropy

*Feray Ünlü, Eunhwan Jung, Senol Öz, Heechae Choi, Thomas Fischer, and Sanjay Mathur**

University of Cologne, Institute of Inorganic Chemistry, Chemistry Department, Greinstr. 6, Cologne, 50939, Germany

1.1 Introduction

The worldwide deployment of photovoltaic technology to combat the growing energy demand often encounters the "golden triangle" of solar technology defined by an optimal balance among cost, efficiency, and stability parameters [1]. During recent years, perovskite-based photoabsorber materials have emerged as a promising alternative for cost-effective and solution-processable photovoltaic devices. The diversity of options related to processing, composition, and device setups makes this research an interesting and rapidly growing domain of energy materials. In particular, methylammonium lead iodide ($CH_3NH_3PbI_3$, $MAPbI_3$), which is the prototype among organic–inorganic hybrid perovskites, represents a semiconductor with a direct band gap of 1.55 eV corresponding to an absorption onset of 800 nm, making it an efficient absorber of the visible light. The photon-generated excitons in $MAPbI_3$ have a weak binding energy of less than 50 meV, which means that most of them can dissociate very rapidly into free carriers at room temperature [2–5]. Compared with organic photoabsorbers, the electrons and holes produced in this material exhibit small effective masses comparable with inorganic Si, resulting in high carrier mobility [6]. The recombination of charge carriers occurs on a timescale of hundreds of nanoseconds, resulting in long carrier-diffusion lengths ranging between 100 and 1000 nm in thin films with thickness less than a micrometer [7]. However, $MAPbI_3$ solar cells lack thermal stability due to the structural transition from tetragonal to cubic phase at 55 °C, which is within the operation window of perovskite solar cells (PSCs). In addition, $MAPbI_3$ compositions tend to degrade under the attack of moisture and oxygen to lose their light harvesting properties. Moreover, fundamental problems such as light-induced trap-state formation are less understood, concerning mainly the reproducibility of devices and posing a barrier on the commercialization of organic–inorganic hybrid perovskites.

* Corresponding author.

Perovskite Solar Cells: Materials, Processes, and Devices, First Edition.
Edited by Shahzada Ahmad, Samrana Kazim, and Michael Grätzel.

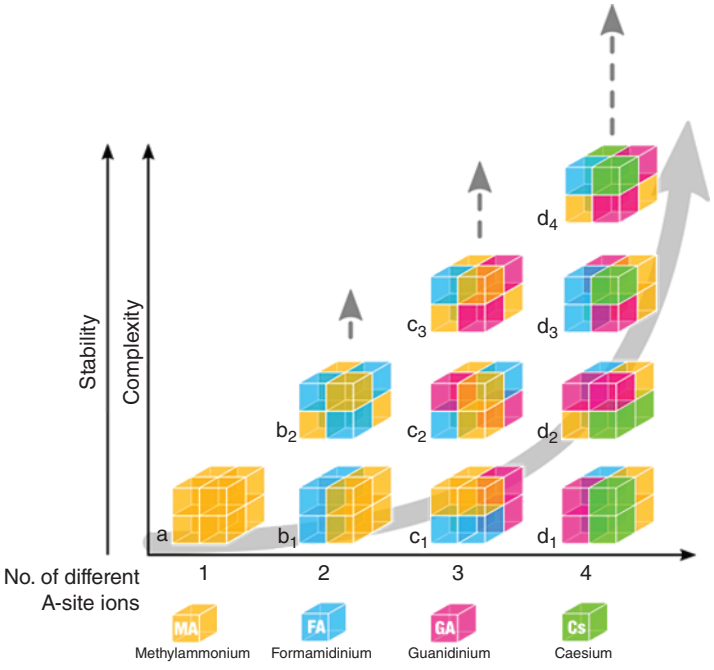

Figure 1.1 The structural complexity of organic–inorganic hybrid perovskites and the related raise of efficiency and stability. Sources: Based on Saliba et al. [8], McMeekin et al. [9], Gong et al. [10].

In this chapter, chemical processing of mixed-cation perovskites based on multiple substitutions on the A-site of the perovskite is discussed in terms of their entropic stability and resulting improvement in the fundamental properties. During the last years, the landscape of synthesis and structure of organic–inorganic perovskites has become more complex due to attempted iterations in compositions to achieve high(er) efficiency and long-term stability of perovskites in photovoltaic (PV) devices. Figure 1.1 schematically illustrates the configurational complexity possible in multiple-cation perovskites that has led to the increased efficiency [8–10]. Nevertheless, the more complex the perovskite, the higher the versatility of functional properties, depending on configurational structure, grain morphology, and optoelectronic properties. Apart from that, an important concept concerning the crystal structure, namely, the Goldschmidt tolerance factor, which allows the prediction of stable crystal phases for certain elements and molecules and their stability, is explained.

1.1.1 Stability Issues of Organic–Inorganic Hybrid Perovskites

Ideal solar modules, which in most cases are placed on the rooftop of the buildings, must be robust against moisture, heat, and light for a long period of time. Despite the high efficiency of PSCs, their long-term stability is still behind the commercial requirements. Although, the organic–inorganic hybrid lead halide perovskites, $MAPbI_3$ and $FAPbI_3$, are excellent semiconductors for PV applications having

demonstrated optimized photovoltaic efficiencies of 21.6% [11] and 25.2% [12], respectively, they are chemically vulnerable against water and superoxide molecules, as well as high intensity light. Especially, moisture is known to initiate the degradation process [13], and various degradation mechanisms have been postulated. However, detailed experimental evidences for a unifying mechanistic model are missing.

Niu et al. [14] reported that the perovskite decomposes back into methylammonium iodide (MAI) and PbI_2 with water (3), HI decomposes from methylamine (4), and after oxidation (5) or under radiation (6), molecular iodine is produced. In other studies, hydrate complexes, or even metallic Pb clusters, are found in degraded perovskite [13], which will not be discussed further here:

$$(3)\ CH_3NH_3PbI_3 \rightleftarrows CH_3NH_3I + PbI_2$$

$$(4)\ CH_3NH_3I \rightleftarrows CH_3NH_2 + HI$$

$$(5)\ HI + O_2 \rightleftarrows 2I_2 + 2H_2O$$

$$(6)\ 2HI \rightleftarrows H_2 + I_2$$

In the case of degradation under light and oxygen, Aristidou et al. [15] claimed that the free electron in the excited $CH_3NH_3PbI_3$ (7) can transfer to oxygen to form superoxide molecule (8), which can deprotonate the MA moiety to release methylamine and iodine (9):

$$(7)\ CH_3NH_3PbI_3 \xrightarrow{h\upsilon} CH_3NH_3PbI_3^*$$

$$(8)\ O_2 \xrightarrow{CH_3NH_3PbI_3^*} O_2^{*-}$$

$$(9)\ CH_3NH_3PbI_3 + O_2^{*-} \xrightarrow{\text{Deprotonation}} CH_3NH_2 + PbI_2 + 1/2I_2 + H_2O$$

Wang et al. [16] investigated the degradation behavior of perovskite polycrystalline films depending on the grain morphology and found that the perovskite single crystals were stable in ambient air for more than two years, which highlights the intrinsic stability of the hybrid perovskites and the effect of grain size and grain boundaries on the stability. Therefore, increased grain sizes were found to show better stability. For instance, thin films with an average grain size of 678 nm showed 10% degradation under humid atmosphere (relative humidity [RH] 85%), whereas 85% degradation occurred for smaller average grain size (297 nm).

Besides the chemical reactions and their implications, the limited thermal instability of perovskites is strongly connected to temperature-driven phase transitions. Pristine $MAPbI_3$ forms the tetragonal phase at room temperature, while a phase transition to the cubic phase occurs at 55 °C, which is within the operating temperature range of a solar cell device and below the surface temperatures (up to 85 °C) generally achieved in the field tests (Figure 1.2). The phase transition not only causes changes in the crystal lattice but also can affect optoelectronic behavior and film morphology. Goldschmidt developed a concept [17] that gives fundamental guidelines to predict stable perovskite structures. Since the phase transitions are strongly related to thermodynamic parameters, the entropy of mixing or configurational entropy plays a critical role in understanding the

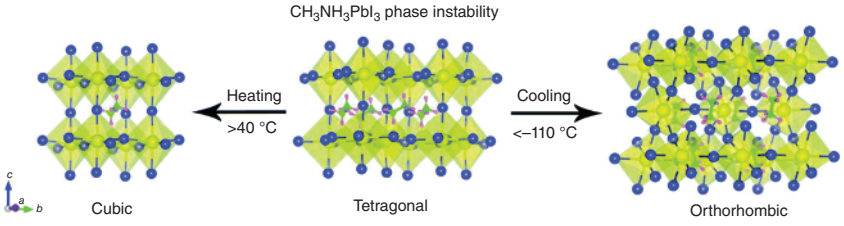

Figure 1.2 Phase transition in $MAPbI_3$ perovskite at different temperatures leads to the phase instability within the solar cell operation frame. Source: Arabpour Roghabadi et al. [13].

structure–property–stability relationship and in designing new perovskites. Section 1.2 briefly reviews the perovskite structure and Goldschmidt's concept revealing the role of A-site cation and its thermodynamic behavior in the lattice. Following this, the chemical processing of multiple-cation perovskites is extensively discussed considering the state of the art of organic–inorganic hybrid perovskite and recent literature reports.

1.2 Crystal Structure of Perovskites

Discovered in 1839 by Gustav Rose and named after Russian mineralogist *Lew Alexejewitsch Perovski*, perovskites represent a family of crystalline compounds that adopt a similar crystal structure as the parent mineral calcium titanate $CaTiO_3$. This class of materials can be generally described by the ABX_3. In the ideal ABX_3 perovskite structure, the large monovalent cation A occupies 12-fold coordination site in the middle of the cube to form an AX_{12} cuboctahedron, while the smaller divalent cation B forms corner sharing BX_6 octahedra in a 3D perovskite framework (Figure 1.3). The ideal cubic perovskite structure is not very common due to the sizes of the cations A and B, and the anion X and the mineral perovskite itself are slightly distorted. Distorted perovskites have reduced symmetry, affecting the

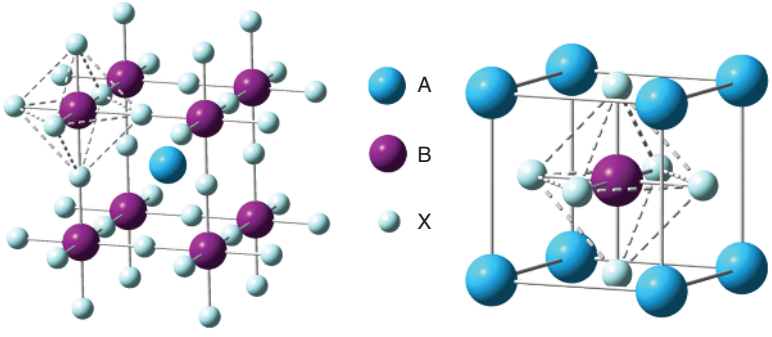

Figure 1.3 The ideal cubic perovskite structure ABX_3 that has a three-dimensional network of corner sharing $[BX_6]$ octahedra surrounding a larger A-site cation.

crystal structure transition, which is one of the key aspects of the structural stability issue for perovskite materials. Such structural distortions, when reversible, can be used for mechanical energy harvesting purposes as demonstrated for the perovskite barium titanate ($BaTiO_3$) [18, 19].

1.2.1 Goldschmidt Tolerance Factor for 3D Structure

In the ideal cubic perovskite structure case, the lattice constant, a, is described in Eqs. (1.1, 1.2):

$$a = \sqrt{2}(r_A + r_X) = 2(r_B + r_X) \tag{1.1}$$

where r_i is the ionic radii of constituting ions (A, B, and X). The ratio of the equations for the lattice constant is given by the Goldschmidt tolerance factor, t, which has been used extensively to predict the stability of the perovskite structure based on chemical formula (ABX_3) and to estimate the degree of distortion [17] that is defined as

$$t = \frac{(r_A + r_X)}{\sqrt{2}(r_B + r_X)} \tag{1.2}$$

It is well known that $t = 1$ stands for a perfect cubic lattice, with the boundary conditions for stable cubic perovskite structures being $0.9 \leq t \leq 1$ and for a distorted perovskite structure being $0.8 \leq t \leq 0.89$, leading to a tetragonal or orthorhombic crystal structure. When the A-site cation is smaller than the ideal value, then t becomes smaller than 1, and as a result the BX_6 octahedra will be distorted to fill space. However, when the A-site cation is too large to form a perovskite structure ($t > 1$), non-perovskite structures such as a hexagonal structure are formed. Similarly, different structures such as ilmenite-type $FeTiO_3$ are formed for $t < 0.8$, when the A-site cation is too small to meet the boundary conditions and form a perovskite structure (Figure 1.4).

The concept of the Goldschmidt tolerance factor works reasonably well with the organic–inorganic halide perovskite materials, which have been used to determine whether a combination of several ions can form a stable perovskite structure [17, 21, 22]. However, there are too many exceptions that cannot be entirely explained by Goldschmidt tolerance factor. Therefore, in such cases, another numerical parameter is necessary to anticipate the structure of a new perovskite configuration especially the substituted ones [23].

1.2.2 Octahedral Factor

The octahedral factor is also known as constraint factor for perovskite structure that is defined as the ratio of the ionic radii of the B-site cation and the halide anion X in the general composition ABX_3 (Eq. (1.3)):

$$\mu = \frac{r_B}{r_X} \tag{1.3}$$

This factor represents the structural stability of the BX_6 octahedron. When it is in the range of $0.44 \leq \mu \leq 0.9$, it generally leads to a stable perovskite structure. Along

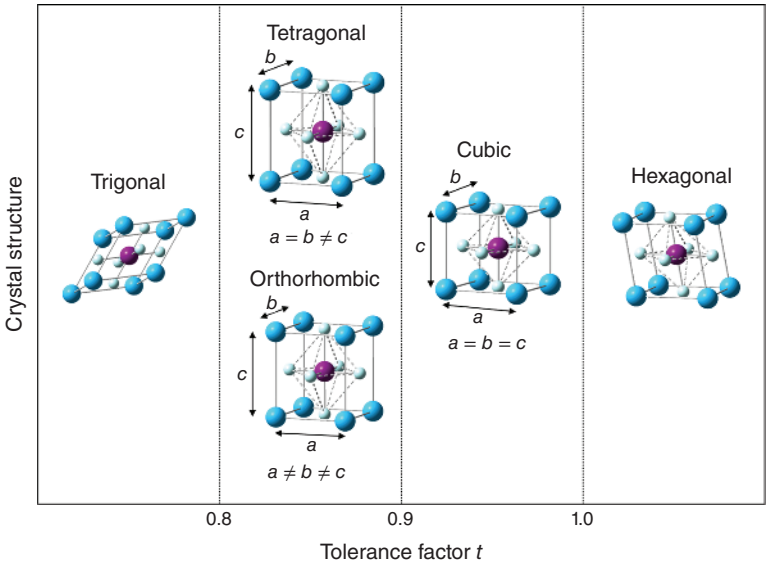

Figure 1.4 The tolerance factor *t* and the crystal structure of perovskite. Source: Adapted from Yu [20].

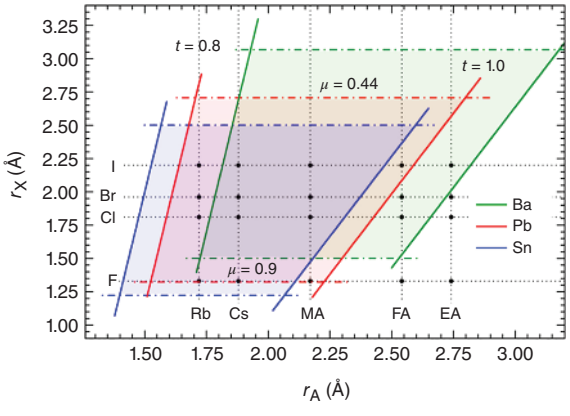

Figure 1.5 Tolerance limit map of parametric space for potentially stable perovskites based on B-site cations Pb, Sn, and Ba. Ionic radii of A-site cations and X-site anions are marked. Source: Yu [20]. Licensed under CC BY 3.0.

with the Goldschmidt tolerance factor, octahedral factor can provide an insight in selecting ions and combinations thereof capable of forming stable halide perovskites among many theoretically possible configurations as indicated in Figure 1.5.

It should be noted that in the case of hybrid perovskites, defining ionic radii for non-symmetric A-site organic molecular cations is nontrivial, and also the reduced electronegativity of heavy halide anions needs to be considered in terms of their polarizability (size/charge) [20, 23]. To address these ambiguities, some modifications have been proposed in elucidating the structural parameters, such as the consideration of effective ionic radii [23].

1.2.3 Role of A-Site Cation

The optoelectronic properties of the hybrid organic–inorganic halide perovskite compounds are strongly governed by the metal halide framework. The valence band is built by the s-lone pair of Pb^{2+} cation and p orbitals of the halide anion, while the conduction band consists of unfilled 6p and 3p orbitals of lead and halogen ions (Figure 1.6). Although the A-site cation does not directly play an important role for the optoelectronic properties [25, 26], the shape, size, and charge distribution of A cations are crucial for forming the perovskite structure. For instance, it was shown that incorporation of a small amount of methylammonium ($A = CH_3NH_3^+$, MA) can stabilize the black phase of perovskite based on formamidinium ($(CH_3(NH_2)_2)^+$, FA), leading to photoconversion efficiencies >20% [27]. The device performance could be improved by addition of an inorganic (Cs^+) or organic ($—C(NH_2)_3^+$, GA) cation that reportedly stabilized the power output of the device as well [8, 10, 28–31].

Highly symmetric cubic structure is the ideal symmetry for enhanced optoelectronic properties of perovskite in which B cation assembled around X anions forms the BX_6 octahedron and A cation occupies the interstitial site (Figure 1.7) [22, 32, 33]. Previous reports showed that there is a dependence between the Goldschmidt tolerance factor and band gap of the perovskite. The higher the tolerance factor ranging $t = 0.8–1.0$, the lower the band gap. However, in the case of GA cation, the compound is not photoactive anymore because it is too large to adopt the perovskite structure.

A-site cations do not directly influence the electronic structure, but they rather play a structure-directing role. The inorganic Pb–I framework is deformed by A-site cation through steric and Coulomb interactions causing an octahedral tilting, which is responsible for the changes in the electronic structure near the band edges. The octahedral tilting and the deviation from the ideal perovskite structure can be

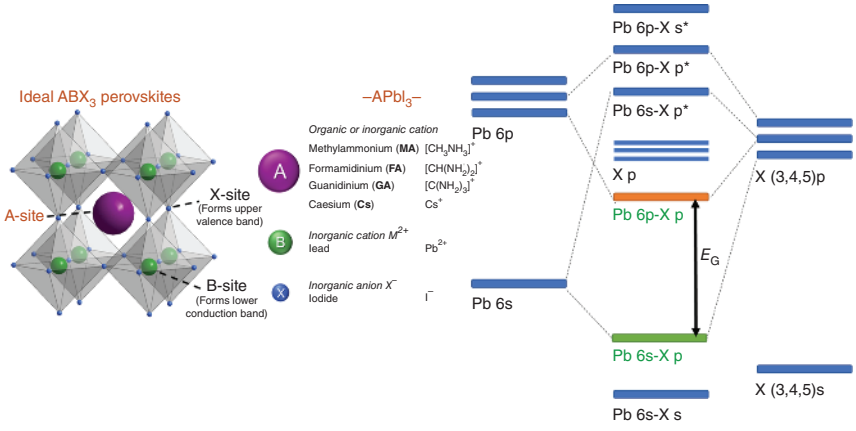

Figure 1.6 The electronic structure of the ideal $APbX_3$ perovskite: valence band (green) consists of s (Pb) and p (halide) orbitals and conduction band (orange) consists of Pb and halide p orbitals, leading to a direct band gap (E_G). Source: Based on Ünlü et al. [24]

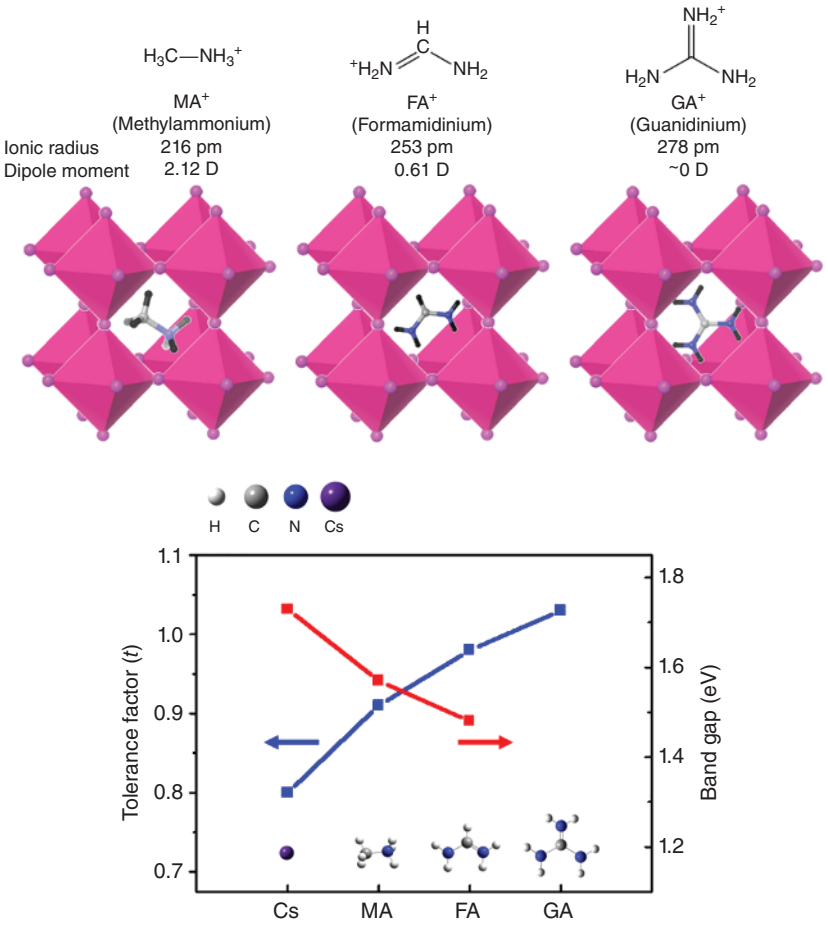

Figure 1.7 Comparison of A-site cations for organic–inorganic hybrid perovskite comparing chemical structure, ionic radius, dipole moment, Goldschmidt tolerance factor, and band gap with schematic structure of the cubic perovskites. Sources: Based on Li et al. [22], Amat et al. [32], Jena et al. [33].

assessed by the octahedra connection bridge Pb–X–Pb angle Φ, which decreases from α-$FAPbI_3$ (Φ = 179.9°) to β-$MAPbI_3$ (Φ = 163.6°) and to γ-$CsPbI_3$ (Φ = 153.2°), resulting in an increase of the band gap of 1.48 eV in α-$FAPbI_3$ to 1.67 eV in γ-$CsPbI_3$ (Figure 1.8). The degree of deviation can be quantified as a function of the angle ψ, which is defined as the average Pb–X–Pb-angle in Pb–X framework. The larger the average Pb–X–Pb angle ψ, the smaller the band gap [34, 35].

1.2.4 Theoretical Calculations: Molecular Dynamics of A-Site Cation

Since the first emergence of the halide PSC [36], a tremendous amount of experimental and theoretical research efforts have been devoted to the engineering and fundamental understanding of PSC [7, 37–43]. On the theoretical side, many of

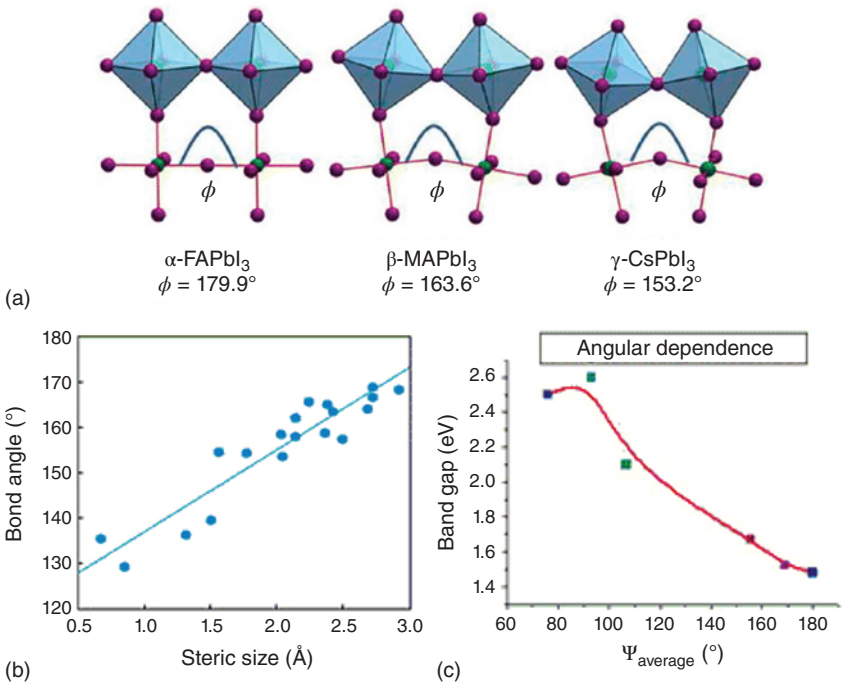

Figure 1.8 Octahedral tilting in the inorganic perovskite lattice because of A-site cation. (a) X–Pb–X angles in organic–inorganic halide perovskites. (b) Bond angle as a function of A-site cation size. Source: Manser et al. [34]. (c) Band-gap dependency from average X–Pb–X bond angle. Source: Stoumpos and Kanatzidis [35].

the intriguing physics hidden in PSC have been explored to discuss the hysteresis, ferroelectricity [40], role of native defects in optical properties [41], Rashba [42], and Dresselhaus [43] effects both in bulk and two-dimensional geometry, prolonged carrier lifetime by rotating methylammonium molecule ions [44], strain-engineered band gap by its unique molecular orbital configuration [45], and so on. These theoretical research work could be mostly done using density functional theory (DFT) [46] calculations, since these are built on quantum mechanical formula and are very appropriate to directly study the orbital-level electronic structures, bond characteristics, and optical transitions.

The simple DFT calculations however often underestimate the perovskite band gaps due to the discontinuity of the exchange–correlation energy, which is a typical shortfall of such techniques [47]. The introduction of relativistic corrections, such as first-order scalar relativistic (SR-DFT) and higher-order spin-orbit coupling effects (SOC-DFT), leads to more realistic values, but these do not exactly match the experimental results. As shown in Figure 1.9, SR-DFT gives nearly similar band gap (E_g) values for $MAPbI_3$ as a result of the compensatory influence of electron self-energy/many-body effects, which tend to increase E_g, and relativistic interactions that reduce E_g. However, it fails to accurately describe the dispersion of the valence band (VB) in Pb perovskites or to calculate exact values for Sn perovskites

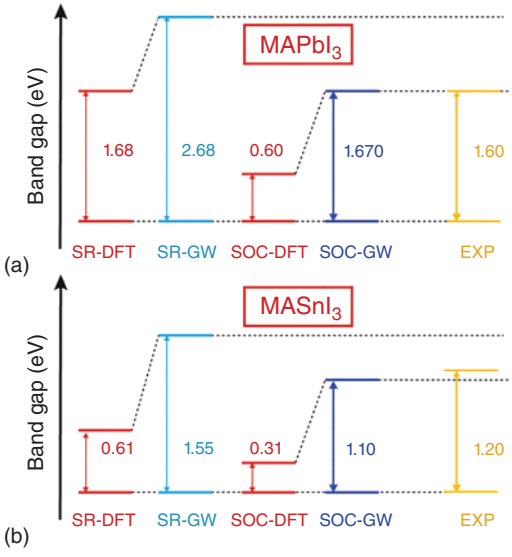

Figure 1.9 Theoretical calculations of perovskites' band gap: comparison of different theoretical methods for (a) $MAPbI_3$ and (b) $MASnI_3$. In both cases, spin-orbit coupling GW (SOC-GW) method could reach better agreement with experimental data. Source: Umari et al. [48].

(Figure 1.9b), as the relativistic effects are less in the lighter metal center. Given the complexity of this system, the state-of-the-art, self-consistent, quasi-particle GW with SOC corrections (spin-orbit coupling quasiparticle self-consistent [SOC-QSGW]) has proven to be the only approach to accurately determine the electronic structure of inorganic and hybrid metal halide perovskites. However, DFT can still provide structural and in some cases semiquantitative information to compare the electronic properties of homologous halide perovskites but should be used with caution [34, 48].

Organic A-site cations show several interesting features, which were investigated in the recent years. For instance, they have a permanent dipole moment, rotate around the C–N axis at their cuboctahedral position, and thus create dynamic and asymmetric structures, which is one of the unique characteristics of organic–inorganic hybrid perovskites compared with their all-inorganic counterparts. The A-site cation interacts with the metal halide framework through Coulomb interactions and hydrogen bonding, influencing the whole perovskite lattice depending on temperature due to the dynamic reorientation [34].

Motta et al. [49] showed through DFT calculations that this dynamic reorientation influences the band structure of the perovskite lattice. They performed DFT calculations for the cubic $MAPbI_3$ considering the fast rotation of MA cation. Therefore, the calculation was not only limited to $CH_3NH_3^+$ in the (100) or (111) direction, for which a higher symmetry is maintained, but also examined cases where the symmetry is reduced. It led to such a symmetry reduction having profound consequences for the electronic structure, namely, that the band gap changes from direct to indirect, when the orientation of the MA cation changes from (111) to (011) orientation (Figure 1.10).

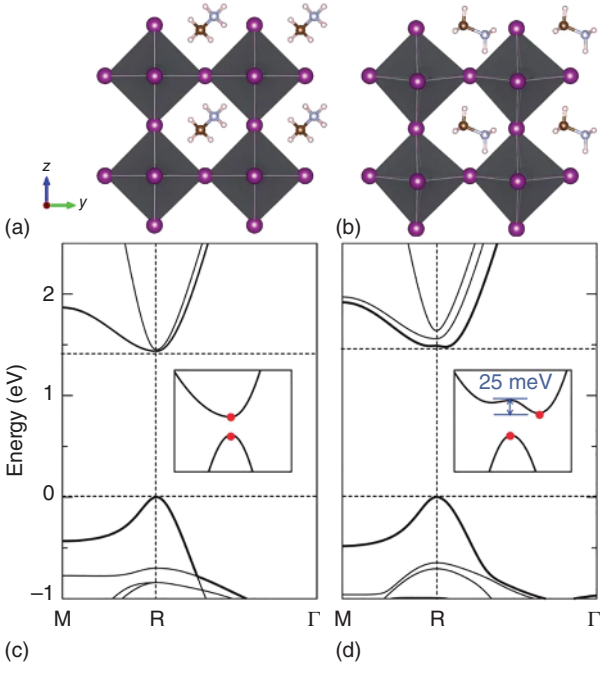

Figure 1.10 Dynamic reorientation of MA cation: cubic $MAPbI_3$ cubic phases with (a) MA in the (111) orientation and (b) in the (011) orientation. Band structures for (c) MA in (111) and (d) in (011) orientation, which shows a band-gap shift from direct to indirect. Source: Motta et al. [49]. Licensed under CC BY 4.0.

1.2.5 Entropy of Mixing: Configurational Effects in Mixed-Cation Perovskites

The configurational entropy of solid materials is related to the way how atoms or molecules are arranged in a mixture, alloy, or crystal lattice. An ideal defect-free and fully ordered material has an entropy of zero. However, this is not the case for real materials where the configurational entropy is defined as "disorder in the site occupancy on crystal sublattices, including defects" [50], and is described with the following equation (Eq. (1.4)), where n is the number of particles and x_n is the mole fraction:

$$S_{\text{conf}} = -nR(x_1 \ln x_1 + x_2 \ln x_2) \tag{1.4}$$

Theoretical calculations and simulations allow to retrieve information on the entropy and enthalpies of systems. In addition, the Goldschmidt's concept including tolerance factor forms the basis to apply DFT methods to obtain deeper insights into the thermodynamics of organic–inorganic hybrid perovskites.

In the case of mixed-cation perovskite, it is important to understand that the perovskite is stable against phase separation. To describe the disorder of mixed-cation

perovskite, the configurational entropy can be introduced. In mixing two components, for instance, $MAPbI_3$ and $FAPbI_3$, the thermodynamic miscibility is given by Helmholtz free energy as function of composition x and temperature T [51] (Eq. (1.5)):

$$\Delta F(x, T) = \Delta U(x, T) - T\Delta S(x, T) \tag{1.5}$$

The internal energy difference of mixed perovskite is defined as

$$\Delta U(x, T) = \frac{\sum_k \Delta U_k(x) g_k e^{-E_k(x)/k_B T}}{\sum_k g_k e^{-E_k(x)/k_B T}} \tag{1.6}$$

$$\Delta U_k(x) = E_k(x) - [(1-x)E_{\mathrm{MAPbI3}} + xE_{\mathrm{FAPbI3}}] \tag{1.7}$$

where E_k is from DFT calculated total energy of the alloy.

The entropy of mixing according to Eq. (1.4) is given by

$$\Delta S(x) = -k_B[x \ln x + (1-x)\ln(1-x)] \tag{1.8}$$

These theoretical calculations can be used to build phase and miscibility diagrams that could eventually support multiple-cation models and explain the alloying experiments.

1.3 Multiple A-Site Cation Perovskites

$MAPbI_3$ is the most popular composition among all organic–inorganic hybrid perovskites, where numerous approaches were reported to optimize structure, morphology of crystals and fabrication of thin films, halide mixing to tune band gap, and crystallization. In contrast to its phase transition at low temperature (>40 °C), formamidinium-based perovskites ($HC(NH_2)_2PbI_3$, $FAPbI_3$) undergo phase transition above 150 °C to form the photoactive black α-phase, which has a lower band gap than $MAPbI_3$ (1.47 vs. 1.55 eV for $MAPbI_3$), and an absorption edge shifted toward the red region allowing the increase of photon absorption and power conversion efficiency (PCE). Yang et al. [52] introduced a direct intramolecular exchange procedure to fabricate $FAPbI_3$ solar cells and observed a PCE of 20.2% and a short-circuit current density (J_{sc}) of 24.7 mA cm^{-2}. However, the black phase of $FAPbI_3$ is not stable at room temperature, at which it forms the inactive yellow δ-phase [53]. Finally, all-inorganic perovskite $CsPbI_3$ is also used in solar cell application due to its higher thermal stability but has a band gap higher (1.73 eV) than the other compositions and active black phase stable at high temperatures (>300 °C). The polymorphism can be controlled by A-site cation engineering to stabilize desired photoactive phase and to tune optical properties and thermal stability. In the following sections, alloying of different A-site cations to reach the configurational stability of hybrid perovskites is presented.

1.3.1 FA^+/MA^+ Alloying for Higher Phase Stability and Photovoltaic Efficiency

Pellet et al. [54] probed the mixing of formamidinium (FA) and methylammonium (MA) cations in 3D hybrid perovskites to expand the absorption spectrum and lower

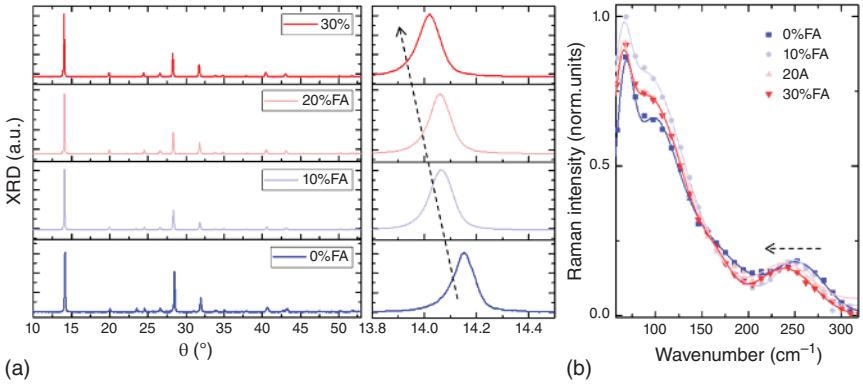

Figure 1.11 Effect of FA/MA alloying on the hybrid perovskite structure. (a) X-ray diffractograms of $FA_xMA_{(1-x)}PbI_3$ thin films showing the peaks shifting to smaller angles while increasing FA amount. (b) Raman intensity of $FA_xMA_{(1-x)}PbI_3$ thin films underlying the shifting related to FA amount. Source: Zhang et al. [55].

the band gap. The combination of A-site cation mixing and sequential deposition method led to phase-pure double-cation black perovskite. Using the double-cation $(MA)_{0.6}(FA)_{0.4}PbI_3$ system, high-performing solar cells could be obtained reaching 14.9% PCE [54]. In their study, Zhang et al. [55] present that by increasing the FA^+ amount into $MAPbI_3$ structure, the photoluminescence (PL) lifetimes increase due to better crystallinity, which leads to reduction of trap states and therefore enhancement of carrier-diffusion length. It was observed that the positions of the diffraction peaks at $2\theta = 14.1°$, 20.0°, 24.4°, 28.4° and 31.8° decreased with increasing FA^+ amount, indicating the enlargement of the crystal lattice to a cubic or quasi-cubic crystal phase (Figure 1.11), giving rise to longer PL lifetimes.

In another approach, where MA^+ was mixed into $FAPbI_3$, Binek et al. [56] have showed that 15% of MA cations are sufficient to stabilize the α-phase at low temperature (Figure 1.12a). They proposed that the intercalation of small-cation MA^+ having high dipole moment enhances the hydrogen bonding to the inorganic Pb–I cage. Moreover, due to better Coulomb interactions between high dipole moment and Pb–I octahedra, the Madelung energy increases, achieving a better stability (Figure 1.12b). In addition, other various chemical methods, e.g. cation exchange [57], mechanosynthesis [58], vapor assisted routes [59], and halide mixing [9, 60], were employed to gain FA/MA-mixed perovskite, aiming at improving grain morphologies, phase purity, and solar cell efficiency.

1.3.2 Cesium Inclusion for Thermal Stability

Apart from the instability of the black phase of $FAPbI_3$ at room temperature, the organic–inorganic hybrid perovskite, although stabilized with $CH_3NH_3^+$ cations, showed lower photostability and thermal stability due to the volatile MA organic moiety. Indeed MA^+ cations induce the crystallization of α-$FAPbI_3$ perovskite, but at a much slower rate due to only slightly smaller size of MA that makes the kinetics sluggish. This leaves a large part of the yellow phase non-transformed.

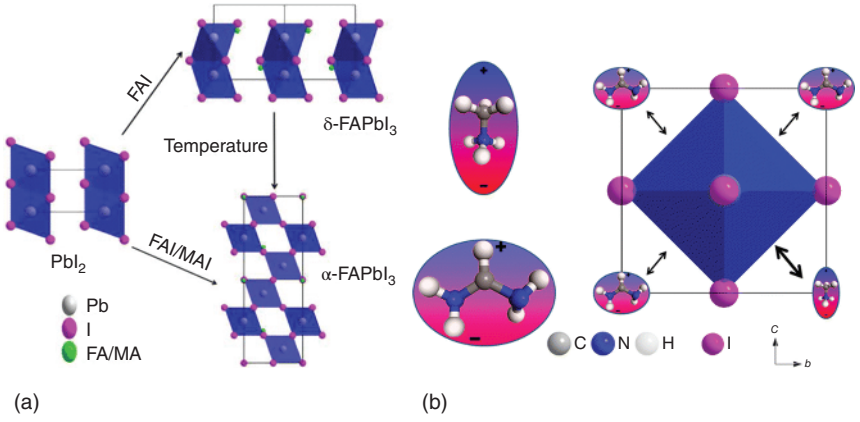

Figure 1.12 Phase stabilization effect of MA/FA alloying. (a) Intercalation of formamidinium iodide (FAI)/MAI in to PbI_2 network leads to the α-phase crystallization of the perovskite, while pure FA-based perovskite forms δ-phase. (b) Optimized structure model of MA-stabilized $FAPbI_3$ showing the different dipole moments and the impact on interaction within the perovskite lattice. Coulomb interaction is stronger in between high dipole moment MA and Pb–I cage. Source: Binek et al. [56].

Alternatively, incorporation of Cs^+ on the A-site of the $FAPbI_3$ or $MAPbI_3$ perovskites could provide better thermal stability and photostability, along with the stabilization of black $FAPbI_3$ at room temperature. The $Cs_{0.1}FA_{0.9}I_3$ turned black even at room temperature with a shrunken perovskite lattice, owing to the smaller cesium cations that led to the reduction of the cuboctahedral A-site vacancy and hence stronger interaction between A-site cation and iodide anions. This reduced A-site volume enables the enhancement in photostability and thermal stability as the FA^+ cations are more enclosed [61]. Furthermore, Cs^+ incorporation lead to larger grains, lower trap states, and longer charge carrier lifetime, improving the solar cell performance to 19% compared with pristine $FAPbI_3$ with PCE of 17.4% [61]. In the case of $Cs_xMA_{1-x}PbI_3$, Niu and coworkers obtained 18.1%, with a J_{SC} of 22.57 mA cm^{-2}, V_{OC} of 1.06 V, and FF of 0.76. In addition, the thermal stability of the unencapsulated devices for $x = 0.09$ was also improved compared with $MAPbI_3$ [62].

Formation of stable cubic perovskite is not favored because $FAPbI_3$ has a larger non-spherical A-site cation, whereas $CsPbI_3$ leads to a smaller tolerance factor (0.81). However, Li and coworkers could show that the alloying of both materials could tune the tolerance factor to a stabilized cubic perovskite structure (Figure 1.13) [22], achieving a new concept to determine effective tolerance factor (Eq. (1.10)):

$$r_{\text{effective}} = xr_A + (1-x)r_B \tag{1.9}$$

$$t_{\text{effective}} = \frac{r_{\text{effective}} + r_X}{\sqrt{2}(r_{Pb^{2+}} + r_X)} \tag{1.10}$$

This methodology in general could be used in finding new perovskites for photostable and thermally stable solar cell applications.

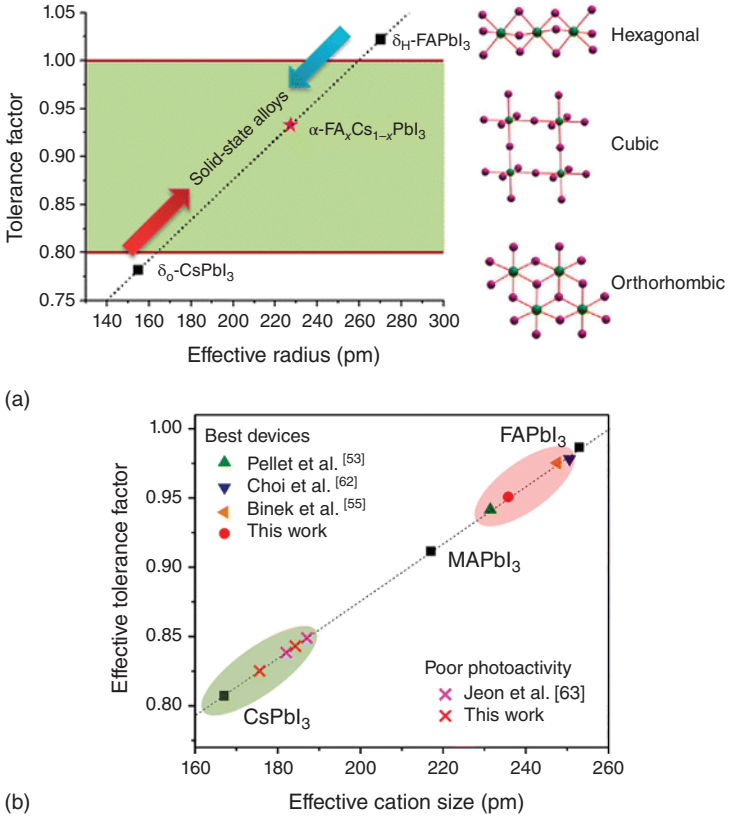

Figure 1.13 Tolerance factor-induced crystallization of perovskites. (a) Combination of small and large cations for tuning of ideal tolerance factor giving cubic structure. (b) Effective tolerance factors obtained from different double-cation perovskites in literature. Source: Li et al. [22].

1.3.3 Rb^+ Small-Cation Influence on Perovskite Structure for Thermal Stability

Apart from cesium cation alloying into $FAPbI_3$, smaller rubidium cations are also suitable for incorporation into the $FAPbI_3$ lattice to maintain the active black phase of formamidinium lead perovskite. However, $RbPbI_3$ forms a yellow δ-phase orthorhombic non-perovskite structure, which is not photoactive probably due to its smaller size that strongly affects the perovskite crystal structure of $FAPbI_3$. Moreover, compared with Cs-containing perovskites, the other advantages are the lower toxicity and better solubility in dimethylformamide, which is commonly used for perovskite solutions. In addition, through the fluorescence lifetime image microscopy (FLIM), Park et al. [65] found that $Rb_{0.05}FA_{0.95}PbI_3$ has longer PL lifetime compared with pristine $FAPbI_3$ due to the suppression of yellow phase formation. The fabricated solar cell exhibited remarkable enhancement of PCE from 13.56% ($FAPbI_3$) to 17.16%, which is related to higher short-circuit current

density (J_{sc}), open-circuit voltage (V_{oc}), and fill factor (FF). The best performing solar cells showed operational stability for 1000 hours under ambient conditions at an average RH of 55% and temperature of 25 °C, maintaining 97% of initial PCE. In contrary, Kubicki et al. [66] claimed that in contrast to Cs that is incorporated in the $FAPbI_3$ lattice, Rb does not form an alloy with FA perovskite. They prepared perovskites via mechanosynthesis and characterized bulk material and thin films with ^{133}Cs and ^{87}Rb solid-state nuclear magnetic resonance spectroscopy (NMR) spectroscopy. In the case of rubidium added to $FAPbI_3$ and to multiple-cation perovskites, it was found to separate into a mixture of rubidium halides acting as passivation layer rather than Rb occupying the position of an interstitial cation.

1.3.4 Guanidinium Large-Cation Influence on Perovskite Structure for Stability

Further attempts to stabilize $MAPbI_3$ or $FAPbI_3$ were made by introducing the larger guanidinium cation ($C(NH_2)_3^+$, GA) into the $MAPbI_3$ lattice. Guanidinium lead iodide ($GAPbI_3$) itself exceeds the limit of tolerance factor ($t = 1.03$), producing low-dimensional perovskites that show temperature-dependent phase instability [67, 68]. However, it has been shown that when GA was incorporated in $MAPbI_3$, 3D structure was maintained in a specific composition range of $MA_{1-x}GA_xPbI_3$ ($0 < x < 0.25$) [69]. As long as the amount of GA was not higher than 25%, 3D structure was maintained without any phase separation of $GAPbI_3$ or $MAPbI_3$ that is thermodynamically less favored. The introduction of small amounts of GA^+ cations led to better stability due to the increased number of H—I bonds, which are shorter (Figure 1.14a). The improvement of H-bonding is also assumed to enhance the grain size and interfacing among grains and further passivation of undercoordinated iodine present within the grain boundaries. This was found to prolong charge carrier lifetimes (Figure 1.14b) and open-circuit voltages (>1.1 V), thus upgrading solar cell performances. In addition, Hou et al. [70] demonstrated the use of guanidinium chloride (GACl) as additive to ameliorate the grain quality of $MAPbI_3$ thin films and for surface passivation and reduced charge recombination.

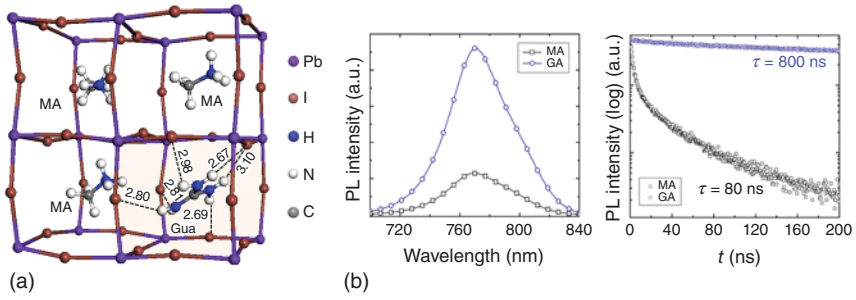

Figure 1.14 (a) Influence of the larger-cation GA on perovskite structure. Source: Jodlowski et al. [69]. Licensed under CC BY 4.0. (b) Enhanced PL lifetimes for mixed GA/MA perovskite compared with pristine $MAPbI_3$. Source: De Marco et al. [30].

They observed that GA does not intercalate into the perovskite crystal lattice, but rather it stays at the grain boundaries to enhance the grain interconnectivity via H-bonds.

1.3.5 Triple- and Quadruple-Cation Hybrid Perovskites for Stability and Optimum Performance

The application of Goldschmidt tolerance factor for 3D perovskites allows not only alloying the two cations on the A-site but also inducing more cations and even having an intermixing of the halide anions. Table 1.1 provides an overview of perovskite compositions used so far, which could achieve high efficiencies through compositional engineering. However, it is theoretically possible to upgrade the solar cell efficiency up to 33% for single-junction PSC depending on the band gap. The Shockley–Queisser limit [78] for best performing single-junction solar cell can be obtained by a semiconductor of 1.34 eV band gap [79]. Among double-cation perovskites, best efficiencies (>20%) could be reached by FA/MA mixing [12, 55, 73, 74]. Although the double-cation strategy could solve some of the problems mentioned, one approach could even outmatch this by using cesium (Cs) as the third A-site cation. Inclusion of Cs^+ in FA/MA perovskite was established by Saliba et al. [8] leading to stable black cubic phase at room temperature without any impurities of the photo inactive δ-phase of $FAPbI_3$. The smaller radius of Cs^+ (1.81 Å) can be employed to decrease the effective tolerance factor and hence gain cubic or pseudo-cubic perovskite structure. The mixed halide triple-cation perovskite $Cs_x(MA_{0.17}FA_{0.83})_{(1-x)}Pb(I_{0.83}Br_{0.17})_3$ yielded stable PCEs above 21% (Figure 1.15b) showing higher thermal stability and reproducibility under several fabrication conditions such as different preparation protocols, temperature and atmospheric changes. This outstanding stability and device reproducibility was an important step towards large-scale application. Singh and Miyasaka [28] could confirm this outstanding property of triple-cation perovskite by its preparation under ambient atmosphere with controlled RH of 25%, achieving stabilized PCE of over 20%. Different antisolvents were used to engineer the grain morphology that showed comparable results, corroborating the insensitivity of the Cs/MA/FA perovskite toward different solvents. The grain size and morphology were affected by Cs concentration under the ambient air process, giving the best performance of device with large micrometer size grains for 5% Cs incorporated in the triple-cation perovskite (Figure 1.15a).

The use of A-site cation engineering enables to increase the entropy of perovskite at the lead site to enlarge the complexity of composition in perovskite, which can stabilize unstable phases of the normal pristine perovskites ($MAPbI_3$, $FAPbI_3$, and $CsPbI_3$). Apart from the abovementioned strategies like mixing two or three cations, the inclusion of further cations can be employed to increase the already achieved stability and charge carrier transport optimizations. Saliba et al. [80] reported on quadruple-cation perovskites employing Rb as fourth cation in their Cs/FA/MA-mixed halide perovskite. Alkali metal cations gained wide interest owing to their stability against oxidation that in turn could stabilize lead- or tin-based perovskites against oxidation. $RbPbI_3$ crystallized in a yellow

Table 1.1 Overview of recently reported highly efficient organic–inorganic multiple A-site cation perovskites with their characteristics.

Perovskite	*t*	Special feature	Record PCE	Stability	References
$MAPbI_3$	0.91	Band gap 1.55 eV High absorption coefficient Low exciton binding energy	21.6%	Fabrication under ambient conditions, room temperature (RT), RH 25%	[11]
$FAPbI_3$	0.99	Band-gap black phase 1.47 eV Broad light harvesting up to 840 nm	25.2%	Certified, 1000 h, RH 20%, retained 90% of PCE	[12]
$CsPbI_3$	0.81	Band-gap black phase 1.73 eV Robust against moisture and air	19.03%	500 h under illumination, retained 90% of PCE	[72]
$FA_{0.1}MA_{0.9}PbI_3$	0.92	Quasi-cubic crystal phase PL redshift Stabilized black phase	20.2%	300 h under full illumination MPP tracking at 45 °C under N_2	[55]
$(FAPbI_3)_{0.92}$ $(MAPbBr_3)_{0.08}$	0.98	Loss in potential of 340 mV EL EQE 8.9% 2D passivation layer on top of perovskite	23.4%	500 h under full illumination MPP tracking, 22.6% PCE (certified), retained 85% of PCE	[73]
$(FAPb_3)_{0.95}$ $(MAPbBr_3)_{0.05}$	0.98	Double-layered solar cell with passivation layer Poly(3-) hexylthiophene HTM	22.7%	200 h, RT, RH 85%, and 1370 h (encapsulated) device under illumination, retained 95% of PCE	[74]
$FA_{0.85}Cs_{0.15}PbI_3$	0.95	Stabilized black cubic phase Band gap 1.52 eV	18.9%	1000 h in air, retained 88% of PCE	[75]
$Cs_{0.05}$ $(MA_{0.17}FA_{0.83})_{1-x}$ $Pb(I_{0.83}Br_{0.17})_3$	0.99	Purer, defect-free perovskite Thermally more stable Highly reproducible	21.1%	250 h under full illumination MPP tracking at RT, 18% PCE (stabilized) Long-lived component 5032 h	[8]
$GA_{0.015}Cs_{0.046}$ $MA_{0.152}FA_{0.787}$ $Pb(I_{0.815}Br_{0.185})_3$	0.97	Bang gap 1.62 eV Long PL lifetime 3.2 µs	20.96%	60 days, under ambient atmosphere at 80 °C, retained 70% of PCE	[76, 77]

Stability is related to the reported conditions during measurements, fabrication, or exclusive stability test. Tolerance factor *t* were calculated according to Eq. (1.3).

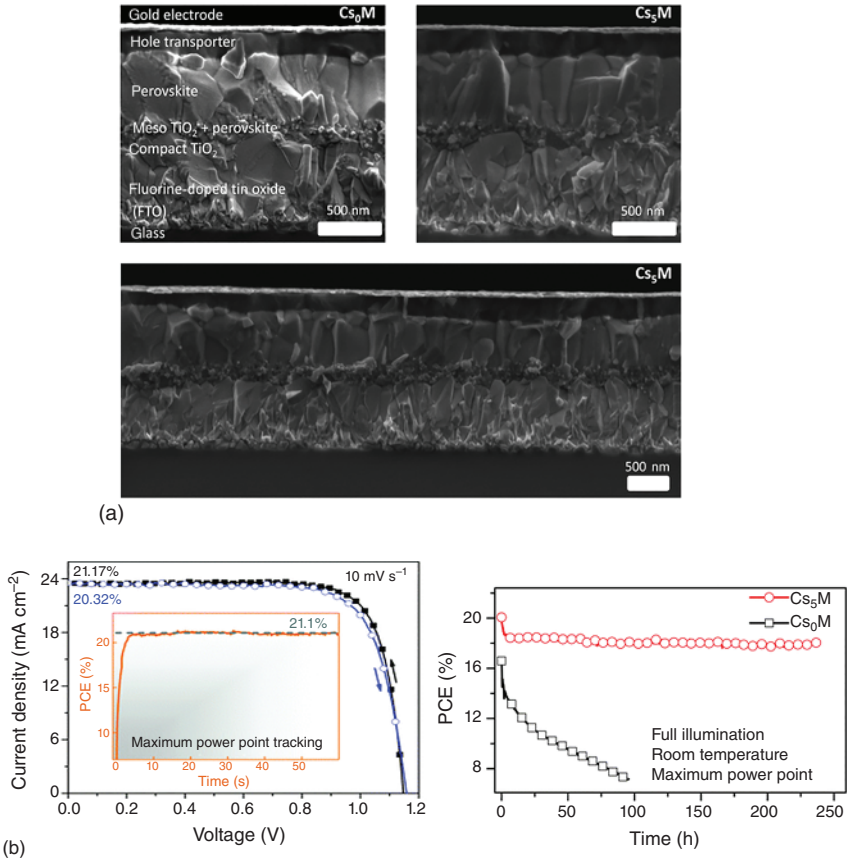

Figure 1.15 Triple- and quadruple-cation hybrid perovskites. (a) Cesium impact on grain morphology of triple-cation Cs/MA/FA perovskites inducing better grain sizes and alignment. (b) Cs/MA/FA-based perovskite solar cells attaining PCE increase and stability under full illumination up to 250 hours of maximum power point (MPP) tracking. Source: (a) Reprinted with the permission from Saliba et al. [8], (b) Saliba et al. [8].

non-perovskite structure with tolerance factor below 0.8. However, with 5% Rb in Rb/Cs/MA/FA, the group could achieve PCE values of over 20.6% with high V_{oc} of 1.24 eV. The loss in potential (difference between V_{oc} and band-gap value) was only 0.39 V, which is due to low nonradiative recombination losses [80]. Theoretically, these values lie between 0.23 V (for band gap of 1.0 eV) and 0.3 V (band gap of 2 eV) for defect-free materials having only radiative recombination [81]. Besides Rb and Cs, the other alkali metals deviate greatly from the ideal tolerance factor, so they are not suitable for intercalation or A-site intermixing. Apart from alkali metal cations,

the inclusion of guanidinium ($C(NH_2)_3^+$, GA) cations in the perovskite was shown to passivate the grain boundaries of thin films to minimize the nonradiative charge carrier recombination and enhance the nonradiative recombination time due to the suppressed formation of halide vacancies [76].

1.3.6 Larger Organic Cations: Reducing Dimensionality for Improved Thermal Stability

Although three-dimensional (3D) hybrid perovskites are preferred due to their excellent optoelectronic properties, the stability issue related to moisture sensitivity remains a challenge toward commercialization. The vulnerability of the prototype compound $MAPbI_3$ against water, which can deprotonate the $CH_3NH_3^+$ moiety to form CH_3NH_2, HI, and PbI_2, is a persisting problem for the environmental stability of perovskites [82–84]. Furthermore, these small organic cations can easily be released at higher temperatures and under illumination [85, 86]. In the context of A-site cation engineering within the 3D perovskite structure, the use of bigger organic cations achieving lower-dimensional perovskite structures seems to be a promising solution against these issues [87]. Since there are no size rules for low-dimensional networked perovskites, A-site cations of different length can be adopted, enabling more flexibility in terms of configurational tuning. Mitzi et al. [88] reported on two-dimensional (2D) layered perovskites with organic ammonium cations ($R—NH_3^+$). Here, the MX_4^{2-} anions are surrounded on both side by organic cations that are stabilized by hydrogen bonds. These layered perovskite structures are analogous to the inorganic *Ruddlesden–Popper* compound K_2NiF_4 (Figure 1.16a) that can be considered as ⟨100⟩ slice of the 3D perovskite structure [88]. Moreover, the 2D layered perovskites are primarily classified into ⟨100⟩, ⟨111⟩, and ⟨110⟩ families (Figure 1.16b), from which the ⟨100⟩ Ruddlesden–Popper (RP) phase is most commonly used for optoelectronic applications. The general formula of RP phase is $(RNH_3)_2\ A_{n-1}BnX_{3n+1}$ where RNH_3 is the organic cation spacer, increasing the lattice of the perovskite due to its larger sizes.

Tsai et al. reported on 2D *Ruddlesden–Popper* perovskite $(BA)_2(MA)_3Pb_4I_{13}$ (BA: *n*-butyl ammonium) with a crystal growth orientation perpendicular to the substrate. This orientation facilitates the charge transport and could yield 12.5% efficiency [89]. Low-dimensional perovskites are generally more stable than 3D perovskites. For example, Smith et al. could fabricate layered perovskite with phenyl ammonium cation, which leads to stability under moisture due to the hydrophobicity of the benzene group [90]. Furthermore, the use of different functional organic spacers, for example, fullerene derivatives, conjugated oligomers, or organic dyes, allows tuning the optoelectronic properties and charge carrier transport abilities of the designed 2D perovskites [91–93]. The size and nature of the organic spacer and the hydrogen bonding to the inorganic frame influence the Pb–I–Pb bond angles, which impact the valence bandwidths where s-orbital (Pb) and p-orbitals have stronger overlap integrals for angles close to 180°, in turn reducing the band gap. Additionally, for 2D perovskites, the interlayer spacing between inorganic layers is the determining factor for band-gap tuning. The longer the interlayer spacing,

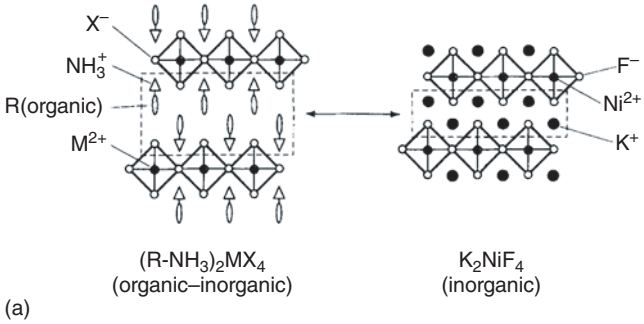

(a)

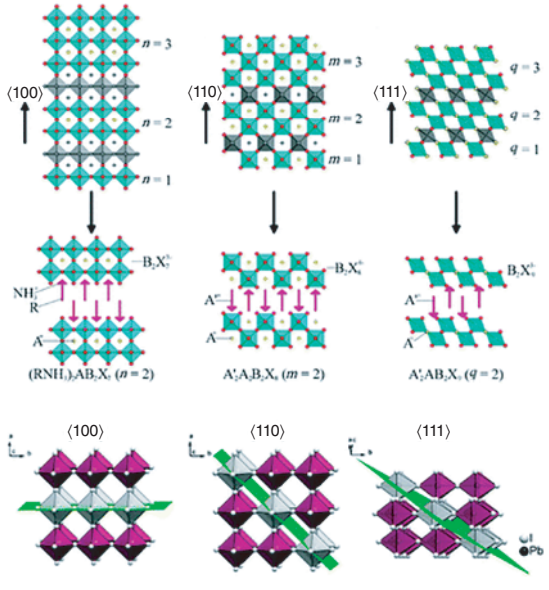

(b)

Figure 1.16 Low-dimensional perovskites. (a) 2D organic–inorganic hybrid perovskites and their similarity to Ruddlesden–Popper compound K_2NiF_4. Source: Mitzi [88]. (b)⟨100⟩, ⟨111⟩, and ⟨110⟩ phases of 2D perovskites. Source: Thrithamarassery Gangadharan and Ma [87].

the wider the band gap. That is why pure 2D layered perovskites could not achieve comparable solar cell performance in relation to the 3D AMX_3 perovskites majorly due to the wider band gaps attributed to bulkier organic spacer cations. Hence, a combination of 2D and 3D perovskites is becoming increasingly interesting in terms of unifying high efficiency and long-term stability in PSCs. In 2D/3D system, the small organic cations are partially replaced by bulkier organic spacer cations. For instance, Grancini et al. [94] reported one-year stable and HTM-free 2D/3D $(AVA)_{0.3}(MA)_{0.7}PbI_3$ (AVA: amino valeric acid, $HOOC(CH_2)_4NH_3$) PSCs, without any obvious loss in efficiency (PCE 12.9%) under ambient air with 1 sun illumination at 55 °C. The partially substitution of the A-site with the organic spacer cation widens the band gap at the interface, which functions as electron recombination barriers due to the lower lying conduction band (CB) of the 2D

perovskite than the CB of the 3D phase. This combination of wide and low band gap perovskites leads to stable power conversion efficiencies of up to 19% for $BA_{0.05}(FA_{0.83}Cs_{0.17})_{0.95}Pb(I_{0.8}Br_{0.2})_3$ designed by Wang et al. [95] The 2D/3D alloying creates heterojunctions inhibiting carrier recombination at grain boundaries consisting of heterodimensional interfaces.

1.4 Conclusion and Perspectives

Organic–inorganic hybrid perovskites gained interest in the past decade, owing to their excellent properties for optoelectronic application such as high absorption coefficient, long carrier lifetimes, and very uniquely the high defect tolerance that allows facile and cheap thin-layer fabrication. Apart from these fundamental characteristics, hybrid perovskites manifested physical and chemical versatilities in terms of crystal structure with various Pb–X framework from 0D to 3D networking, achieving a wide scope of application opportunities, e.g. solar cells, light-emitting diodes, photodetectors, or ferroelectrics. Moreover, the dynamic organic A-site cations lead to a great flexibility of the perovskite lattice compared with the classical inorganic oxide perovskites. Altogether, hybrid perovskites developed as highly efficient new technology and can be the next-generation solar technology. To fulfill the requirements for commercialization of PSCs, the stability is recently the most important challenge, which researchers address.

The formation of an intrinsic stable perovskite structure can be predicted by the concept of Goldschmidt's tolerance factor, allowing the versatility of elements in the sites of the ABX_3 framework if complied with $0.9 < t < 1$ [33]. A very important approach to overcome the phase instability and thermal instability was the chemical processing of multiple-cation perovskites. The controlled alloying of various cations at the A-site of the ABX_3 perovskite could enhance the stability of the usually sensitive $MAPbI_3$ perovskite toward phase transition and moisture. The main role of this cation is to template the perovskite inorganic framework and thus influence the electronic structure indirectly. Especially organic polar A-site cations, which rotate within the inorganic frame, lead to a dynamic disorder [96–98]. This could be controlled by alloying inorganic cations such as Cs and Rb into the multiple-cation perovskite [65, 80, 99–101].

To provide external stability, great efforts have been made to improve the moisture resistance of the vulnerable perovskite layers, either by incorporating hydrophobic layers such as polymers/carbon composites [102], by incorporating non-hygroscopic intermediate layers between perovskite and hole transport material (HTM) [103, 104], or by passivating the perovskite surface by small molecules [105, 106]. Furthermore, lowering the dimensionality of the inorganic octahedral network by large organic A-site cations turned out to be a possible solution for the stability issue [87, 94, 95].

Apart from organic–inorganic hybrid perovskites, all-inorganic lead halide perovskites have emerged as an important class of strongly emissive materials with promising applications in PV, photodetectors, and light-emitting diodes (LEDs).

$CsPbX_3$ materials exhibit several advantages, including higher melting point (>500 °C), higher thermal stability, and higher stability against photobleaching, making them suitable candidates for optoelectronic applications [107]. Therefore, $CsPbX_3$ nanocrystal colloids have become the most popular perovskite studied for LED applications. For PV applications, $CsPbX_3$ perovskites have also recently made great progress in terms of efficiency, reaching over 18% [108].

Apart from PSCs, perovskite-based LEDs also gained interest in recent years, achieving a quantum efficiency of above 20% (in comparison with 30% reported for best performing organic LEDs) in about four years. Moreover, the flexibility in perovskite material composition allows to tune the exciton emissions in the desired wavelength region that decides the emissive color [109]. The major issues with perovskite LEDs at the present stage of progress are material stability/thermal stability, which is being addressed by all-inorganic perovskites, and color stability, i.e. color changing with duration of operation under the constant voltage, likely due to ion migration and operational stability, required as a standard evaluation for successful commercialization. Surface defect passivation and interface engineering will be the approaches used to enhance the performance of both PV and LED technologies [110].

Organic–inorganic hybrid perovskites and their all-inorganic $CsPbX_3$ counterparts stand out due to their excellent optoelectronic properties, which have been improved immensely by a wide variety of methods worldwide within a remarkably short time. Due to the variation in the composition, problems such as structural instability could be eliminated. Interface engineering has made it possible to produce not only highly efficient solar cells but also solar cell stability in laboratories up to 1000 hours. However, for commercialization, other important factors play an important role. Apart from structure-based intrinsic stability, which could be eliminated so far by this A-site cation engineering, other reasons caused by ion migration, defect dynamics, thermal strain between substrate and perovskite film, crystal strain, and crystal orientation should be investigated more extensively.

The commercial feasibility of emerging generation technologies such as PSCs also depends on improved costs per watt peak (Wp) of the installation compared with the already used classical PV technology on the market [111]. The outstanding advantage of PSCs is the possible use of solution-based techniques at low temperatures such as spraying, doctor blading, and roll-to-roll printing and the promise of highly efficient, lightweight, and low-cost options, leading to the reasonable energy payback times.

Now there are two main challenges in this area: fundamental understanding of the physics, chemistry, and engineering of perovskite technology and scaling up and optimization of the production toward commercialization. For this, it is not only important to optimize thin-film fabrication or achieve high efficiencies. Today, it is rather important to comply with the general restrictions, such as more sustainable large-scale production. One small step toward more sustainable fabrication could be the avoidance of toxic and environmentally harmful solvents, which are mainly used in perovskite thin-film fabrication.

Meanwhile, our group has established protic ionic liquids (PILs) in solution-based hybrid perovskite processing [27], which resulted in a substantial decrease of annealing temperature and time required for the formation of polycrystalline perovskite thin films without compromising the final film quality. Furthermore, it was possible to use green solvents such as water, alcohols, or acetonitrile. However, we further aim to focus on the development of such perovskite inks including the fundamental investigation of solution dynamics.

Acknowledgments

The financial and infrastructural support provided by the University of Cologne is thankfully acknowledged. The German Science Foundation (DFG) is gratefully acknowledged for the project funding received within the priority programme SPP 2196 "Perovskite semiconductors: From fundamental properties to devices" and in the frame of the SPP 1959 "Manipulation of matter controlled by electric and magnetic field: Towards novel synthesis and processing routes of inorganic materials."

References

1 Snaith, H. and Perovskites, J. (2013). The emergence of a new era for low-cost, high-efficiency solar cells. *J. Phys. Chem. Lett.* 4: 3623–3630.
2 Miyata, A., Mitioglu, A., Plochocka, P. et al. (2015). Direct measurement of the exciton binding energy and effective masses for charge carriers in organic-inorganic tri-halide perovskites. *Nat. Phys.* 11: 582–587.
3 Hirasawa, M., Ishihara, T., Goto, T. et al. (1994). Magnetoabsorption of the lowest exciton in perovskite-type compound $(CH_3NH_3)PbI_3$. *Phys. B Phys. Condens. Matter* 201: 427–430.
4 D'Innocenzo, V., Grancini, G., Alcocer, M.J.P. et al. (2014). Excitons versus free charges in organo-lead tri-halide perovskites. *Nat. Commun.* 5: 1–6.
5 Valverde-Chávez, D.A., Ponseca, C.S., Stoumpos, C.C. et al. (2015). Intrinsic femtosecond charge generation dynamics in single crystal $CH_3NH_3PbI_3$. *Energy Environ. Sci.* 8: 3700–3707.
6 Giorgi, G., Fujisawa, J.I., Segawa, H., and Yamashita, K. (2013). Small photocarrier effective masses featuring ambipolar transport in methylammonium lead iodide perovskite: a density functional analysis. *J. Phys. Chem. Lett.* 4: 4213–4216.
7 Cui, J., Yuan, H., Li, J. et al. (2015). Recent progress in efficient hybrid lead halide perovskite solar cells. *Sci. Technol. Adv. Mater.* 16: 036004.
8 Saliba, M., Matsui, T., Seo, J.Y. et al. (2016). Cesium-containing triple cation perovskite solar cells: improved stability, reproducibility and high efficiency. *Energy Environ. Sci.* 9: 1989–1997.

9 McMeekin, D.P., Sadoughi, G., Rehman, W. et al. (2016). A mixed-cation lead mixed-halide perovskite absorber for tandem solar cells. *Science (80-.)* 351: 151–155.

10 Gong, J., Guo, P., Benjamin, S.E. et al. (2018). Cation engineering on lead iodide perovskites for stable and high-performance photovoltaic applications. *J. Energy Chem.* 27: 1017–1039.

11 Kogo, A., Sanehira, Y., Numata, Y. et al. (2018). Amorphous metal oxide blocking layers for highly efficient low-temperature brookite TiO_2-based perovskite solar cells. *ACS Appl. Mater. Interfaces* 10: 2224–2229.

12 Jeon, J., Kim, M., Seo, J. et al. (2021). Pseudo-halide anion engineering for α-$FAPbI_3$ perovskite solar cells. *Nature* 592 (7854): 381–385.

13 Arabpour Roghabadi, F., Alidaei, M., Mousavi, S.M. et al. (2019). Stability progress of perovskite solar cells dependent on the crystalline structure: from 3D ABX3 to 2D Ruddlesden–Popper perovskite absorbers. *J. Mater. Chem. A* 7: 5898–5933.

14 Niu, G., Li, W., Meng, F. et al. (2014). Study on the stability of $CH_3NH_3PbI_3$ films and the effect of post-modification by aluminum oxide in all-solid-state hybrid solar cells. *J. Mater. Chem. A* 2: 705–710.

15 Aristidou, N., Sanchez-Molina, I., Chotchuangchutchaval, T. et al. (2015). The role of oxygen in the degradation of methylammonium lead trihalide perovskite photoactive layers. *Angew. Chem. Int. Ed.* 54: 8208–8212.

16 Wang, Q., Chen, B., Liu, Y. et al. (2017). Scaling behavior of moisture-induced grain degradation in polycrystalline hybrid perovskite thin films. *Energy Environ. Sci.* 10: 516–522.

17 Goldschmidt, V.M. (1926). Die Gesetze der Krystallochemie. *Naturwissenschaften* 14: 477–485.

18 Acosta, M., Novak, N., Rojas, V. et al. (2017). $BaTiO_3$-based piezoelectrics: fundamentals, current status, and perspectives. *Appl. Phys. Rev.* 4: 041305.

19 Burns, G. and Dacol, F.H. (1982). Polarization in the cubic phase of $BaTIO_3$. *Solid State Commun.* 42: 9. https://doi.org/10.1016/0038-1098(82)91018-3.

20 Yu, C.-J. (2019). Advances in modelling and simulation of halide perovskites for solar cell applications. *J. Phys. Energy* 1: 022001.

21 Ji, D., Feng, S.Z., Wang, L. et al. (2019). Regulatory tolerance and octahedral factors by using vacancy in $APbI_3$ perovskites. *Vacuum* 164: 186–193.

22 Li, Z., Yang, M., Park, J.S. et al. (2016). Stabilizing perovskite structures by tuning tolerance factor: formation of formamidinium and cesium lead iodide solid-state alloys. *Chem. Mater.* 28: 284–292.

23 Kieslich, G., Sun, S., and Cheetham, A.K. (2015). An extended tolerance factor approach for organic–inorganic perovskites. *Chem. Sci.* 6: 3430–3433.

24 Ünlü, F., Jung, E., Haddad, J. et al. (2020). Understanding the interplay of stability and efficiency in A-site engineered lead halide perovskites. *APL Mater.* 8 (7): 070901.

25 Chang, Y.H., Park, C.H., and Matsuishi, K. (2004). First-principles study of the structural and the electronic properties of the lead-halide-based

inorganic–organic perovskites (CH_3 NH_3) PbX_3 and $CsPbX_3$ (X = Cl, Br, I). *J. Korean Phys. Soc.* 44: 889–893.

26 Umebayashi, T., Asai, K., Kondo, T., and Nakao, A. (2003). Electronic structures of lead iodide based low-dimensional crystals. *Phys. Rev. B – Condens. Matter Mater. Phys.* 67: 2–7.

27 Öz, S., Burschka, J., Jung, E. et al. (2018). Protic ionic liquid assisted solution processing of lead halide perovskites with water, alcohols and acetonitrile. *Nano Energy* 51: 632–638.

28 Singh, T. and Miyasaka, T. (2018). Stabilizing the efficiency beyond 20% with a mixed cation perovskite solar cell fabricated in ambient air under controlled humidity. *Adv. Energy Mater.* 8: 1–9.

29 Giorgi, G. and Yamashita, K. (2015). Zero-dipole molecular organic cations in mixed organic-inorganic halide perovskites: possible chemical solution for the reported anomalous hysteresis in the current-voltage curve measurements. *Nanotechnology* 26: 442001.

30 De Marco, N., Zhou, H., Chen, Q. et al. (2016). Guanidinium: a route to enhanced carrier lifetime and open-circuit voltage in hybrid perovskite solar cells. *Nano Lett.* 16: 1009–1016.

31 Kubicki, D.J., Prochowicz, D., Hofstetter, A. et al. (2018). Formation of stable mixed guanidinium-methylammonium phases with exceptionally long carrier lifetimes for high-efficiency lead iodide-based perovskite photovoltaics. *J. Am. Chem. Soc.* 140: 3345–3351.

32 Amat, A., Mosconi, E., Ronca, E. et al. (2014). Cation-induced band-gap tuning in organohalide perovskites: interplay of spin-orbit coupling and octahedra tilting. *Nano Lett.* 14: 3608–3616.

33 Jena, A.K., Kulkarni, A., and Miyasaka, T. (2019). Halide perovskite photovoltaics: background, status, and future prospects. *Chem. Rev.* 119: 3036–3103.

34 Manser, J.S., Christians, J.A., and Kamat, P.V. (2016). Intriguing optoelectronic properties of metal halide perovskites. *Chem. Rev.* 116: 12956–13008.

35 Stoumpos, C.C. and Kanatzidis, M.G. (2015). The renaissance of halide perovskites and their evolution as emerging semiconductors. *Acc. Chem. Res.* 48: 2791–2802.

36 Kojima, A., Teshima, K., Shirai, Y., and Miyasaka, T. (2009). Organometal halide perovskites as visible- light sensitizers for photovoltaic cells. *J. Am. Chem. Soc.* 131: 6050–6051.

37 Hariz, A. (2016). Perspectives on organolead halide perovskite photovoltaics. *J. Photonics Energy* 6: 032001.

38 Ivanovska, T., Dionigi, C., Mosconi, E. et al. (2017). Long-lived photoinduced polarons in organohalide perovskites. *J. Phys. Chem. Lett.* 8: 3081–3086.

39 Khenkin, M.V., Anoop, K.M., Visoly-Fisher, I. et al. (2018). Reconsidering figures of merit for performance and stability of perovskite photovoltaics. *Energy Environ. Sci.* 11: 739–743.

40 Yuan, Y., Xiao, Z., Yang, B., and Huang, J. (2014). Arising applications of ferroelectric materials in photovoltaic devices. *J. Mater. Chem. A* 2: 6027–6041.

41 Kim, J., Lee, S.H., Lee, J.H., and Hong, K.H. (2014). The role of intrinsic defects in methylammonium lead iodide perovskite. *J. Phys. Chem. Lett.* 5: 1312–1317.

42 Zhai, Y., Baniya, S., Zhang, C. et al. (2017). Giant Rashba splitting in 2D organic-inorganic halide perovskites measured by transient spectroscopies. *Sci. Adv.* 3: 1–7.

43 Kepenekian, M. and Even, J. (2017). Rashba and Dresselhaus couplings in halide perovskites: accomplishments and opportunities for spintronics and spin-orbitronics. *J. Phys. Chem. Lett.* 8: 3362–3370.

44 Chen, T., Chen, W.-L., Foley, B.J. et al. (2017). Origin of long lifetime of band-edge charge carriers in organic–inorganic lead iodide perovskites. *Proc. Natl. Acad. Sci.* 114: 7519–7524.

45 Kim, J., Lee, S.H., Chung, C.H., and Hong, K.H. (2016). Systematic analysis of the unique band gap modulation of mixed halide perovskites. *Phys. Chem. Chem. Phys.* 18: 4423–4428.

46 Kohn, W. and Sham, L.J. (1965). Self-consistent equations including exchange and correlation effects. *Physiol. Rev.* 140: A1133.

47 Perdew, J.P. (1985). Density functional theory and the band gap problem. *Int. J. Quantum Chem.* 28: 497–523.

48 Umari, P., Mosconi, E., and De Angelis, F. (2014). Relativistic GW calculations on $CH_3NH_3PbI_3$ and $CH_3NH_3SnI_3$ perovskites for solar cell applications. *Sci. Rep.* 4: 4467.

49 Motta, C., El-Mellouhi, F., Kais, S. et al. (2015). Revealing the role of organic cations in hybrid halide perovskite $CH_3NH_3PbI_3$. *Nat. Commun.* 6: 7026.

50 Butler, K.T., Walsh, A., Cheetham, A.K., and Kieslich, G. (2016). Organised chaos: entropy in hybrid inorganic-organic systems and other materials. *Chem. Sci.* 7: 6316–6324.

51 Brivio, F., Caetano, C., and Walsh, A. (2016). Thermodynamic origin of photoinstability in the $CH_3NH_3Pb(I_{1-x}Br_x)_3$ hybrid halide perovskite alloy. *J. Phys. Chem. Lett.* 7: 1083–1087.

52 Yang, W.S., Noh, J.H., Jeon, N.J. et al. (2015). High-performance photovoltaic perovskite layers fabricated through intramolecular exchange. *Science* 348 (6240): 1234–1237.

53 Koh, T.M., Fu, K., Fang, Y. et al. (2014). Formamidinium-containing metal-halide: an alternative material for near-IR absorption perovskite solar cells. *J. Phys. Chem. C* 118: 16458–16462.

54 Pellet, N., Gao, P., Gregori, G. et al. (2014). Mixed-organic-cation perovskite photovoltaics for enhanced solar-light harvesting. *Angew. Chem. Int. Ed.* 53: 3151–3157.

55 Zhang, Y., Grancini, G., Feng, Y. et al. (2017). Optimization of stable quasi-cubic $FA_xMA_{1-x}PbI_3$ perovskite structure for solar cells with efficiency beyond 20%. *ACS Energy Lett.* 2: 802–806.

56 Binek, A., Hanusch, F.C., Docampo, P., and Bein, T. (2015). Stabilization of the trigonal high-temperature phase of formamidinium lead iodide. *J. Phys. Chem. Lett.* 6: 1249–1253.

57 Ji, F., Wang, L., Pang, S. et al. (2016). A balanced cation exchange reaction toward highly uniform and pure phase FA1: XMA_xPbI_3 perovskite films. *J. Mater. Chem. A* 4: 14437–14443.

58 Prochowicz, D., Yadav, P., Saliba, M. et al. (2017). Mechanosynthesis of pure phase mixed-cation MA: $XFA_{1-x}PbI_3$ hybrid perovskites: photovoltaic performance and electrochemical properties. *Sustain. Energy Fuels* 1: 689–693.

59 Chen, J., Xu, J., Xiao, L. et al. (2017). Mixed-organic-cation $(FA)_x$ $(MA)_{1-x}PbI_3$ planar perovskite solar cells with 16.48% efficiency via a low-pressure vapor-assisted solution process. *ACS Appl. Mater. Interfaces* 9: 2449–2458.

60 Isikgor, F.H., Li, B., Zhu, H. et al. (2016). High performance planar perovskite solar cells with a perovskite of mixed organic cations and mixed halides, $MA_{1-x}FA_xPbI_{3-y}Cl_y$. *J. Mater. Chem. A* 4: 12543–12553.

61 Lee, J.W., Kim, D.-H., Kim, H.-S. et al. (2015). Formamidinium and cesium hybridization for photo- and moisture-stable perovskite solar cell. *Adv. Energy Mater.* 5: 1501310.

62 Niu, G., Li, W., Li, J. et al. (2017). Enhancement of thermal stability for perovskite solar cells through cesium doping. *RSC Adv.* 7: 17473–17479.

63 Choi, H., Jeong, J., Kim, H. et al. (2014). Cesium-doped methylammonium lead iodide perovskite light absorber for hybrid solar cells. *Nano Energy* 7: 80–85.

64 Jeon, N.J., Noh, J.H., Yang, W.S. et al. (2015). Compositional engineering of perovskite materials for highperformance solar cells. *Nature* 517: 476–480.

65 Park, Y.H., Jeong, I., Bae, S. et al. (2017). Inorganic rubidium cation as an enhancer for photovoltaic performance and moisture stability of $HC(NH_2)_2PbI_3$ perovskite solar cells. *Adv. Funct. Mater.* 27: 21–27.

66 Kubicki, D.J., Prochowicz, D., Hofstetter, A. et al. (2017). Phase segregation in Cs-, Rb- and K-doped mixed-cation $(MA)_x(FA)_{1-x}PbI_3$ hybrid perovskites from solid-state NMR. *J. Am. Chem. Soc.* 139: 14173–14180.

67 Szafrański, M. (1997). Investigation of phase instabilities in guanidinium halogenoplumbates(II). *Thermochim. Acta* 307: 177–183.

68 Szafrański, M. and Katrusiak, A. (2000). Phase transitions in the layered structure of diguanidinium tetraiodoplumbate. *Phys. Rev. B: Condens. Matter Mater. Phys.* 61: 1026–1035.

69 Jodlowski, A.D., Roldán-Carmona, C., Grancini, G. et al. (2017). Large guanidinium cation mixed with methylammonium in lead iodide perovskites for 19% efficient solar cells. *Nat. Energy* 2: 972–979.

70 Hou, X., Hu, Y., Liu, H. et al. (2017). Effect of guanidinium on mesoscopic perovskite solar cells. *J. Mater. Chem. A* 5: 73–78.

71 Jeong, M., Choi, I.W., and Go, E.M. (2020). Stable perovskite solar cells with efficiency exceeding 24.8% and 0.3-V voltage loss. *Science (80-.)* 369: 1615–1620.

72 Wang, Y., Liu, X., and Zhang, T. (2019). The role of dimethylammonium iodide in $CsPbI_3$ perovskite fabrication: additive or dopant? *Angew. Chem. Int. Ed.* 58: 16691–16696.

73 Yoo, J.J., Wieghold, S., Sponseller, M.C. et al. (2019). An interface stabilized perovskite solar cell with high stabilized efficiency and low voltage loss. *Energy Environ. Sci.* 12: 2192–2199.

74 Jung, E.H., Jeon, N.J., Park, E.Y. et al. (2019). Efficient, stable and scalable perovskite solar cells using poly(3-hexylthiophene). *Nature* 567: 511–515.

75 Li, N., Liu, J., and Li, C. (2020). Zwitterion-stabilizing scalable bladed α-phase $Cs_{0.1}FA_{0.9}PbI_3$ films for efficient inverted planar perovskite solar cells. *ACS Sustainable Chem. Eng.* 8: 7020–7030.

76 Jung, E., Budzinauskas, K., Öz, S. et al. (2020). Femto-to microsecond dynamics of excited electrons in a quadruple cation perovskite. *ACS Energy Lett.*: 785–792. https://doi.org/10.1021/acsenergylett.9b02684.

77 Zhang, W., Xiong, J., Li, J., and Daoud, W.A. (2019). Guanidinium induced phase separated perovskite layer for efficient and highly stable solar cells. *J. Mater. Chem. A* 7: 9486–9496.

78 Shockley, W. and Queisser, H.J. (1961). Detailed balance limit of efficiency of p–n junction solar cells. *J. Appl. Phys.* 32: 510–519.

79 Rühle, S. (2016). Tabulated values of the Shockley–Queisser limit for single junction solar cells. *Sol. Energy* 130: 139–147.

80 Saliba, M., Matsui, T., Domanski, K. et al. (2016). Incorporation of rubidium cations into perovskite solar cells improves photovoltaic performance. *Science (80-.)* 354.

81 Green, M.A. (2012). Radiative efficiency of state-of-the-art photovoltaic cells. *Prog. Photovoltaics Res. Appl.* 20: 472–476.

82 Niu, G., Guo, X., and Wang, L. (2015). Review of recent progress in chemical stability of perovskite solar cells. *J. Mater. Chem. A* 3: 8970–8980.

83 Manser, J.S., Saidaminov, M.I., Christians, J.A. et al. (2016). Making and breaking of lead halide perovskites. *Acc. Chem. Res.* 49: 330–338.

84 Juarez-Perez, E.J., Ono, L.K., Maeda, M. et al. (2018). Photodecomposition and thermal decomposition in methylammonium halide lead perovskites and inferred design principles to increase photovoltaic device stability. *J. Mater. Chem. A* 6: 9604–9612.

85 Aristidou, N., Eames, C., Sanchez-Molina, I. et al. (2017). Fast oxygen diffusion and iodide defects mediate oxygen-induced degradation of perovskite solar cells. *Nat. Commun.* 8: 1–10.

86 Xiang, Y., Zhang, F., He, J. et al. (2018). Light-current-induced acceleration of degradation of methylammonium lead iodide perovskite solar cells. *J. Power Sources* 384: 303–311.

87 Thrithamarassery Gangadharan, D. and Ma, D. (2019). Searching for stability at lower dimensions: current trends and future prospects of layered perovskite solar cells. *Energy Environ. Sci.* 12: 2860–2889.

88 Mitzi, D. and Synthesis, B. (1999). Structure , and properties of organic-inorganic perovskites and related materials. *Prog. Inorg. Chem.* 48: 1–121.

89 Tsai, H. and Nie, W. (2016). High-efficiency two-dimensional Ruddlesden–Popper perovskite solar cells. *Nature* 536: 312–316.

90 Smith, I.C., Hoke, E.T., Solis-Ibarra, D. et al. (2014). A layered hybrid perovskite solar-cell absorber with enhanced moisture stability. *Angew. Chem. Int. Ed.* 53: 11232–11235.

91 Leveillee, J., Katan, C., Zhou, L. et al. (2018). Influence of π-conjugated cations and halogen substitution on the optoelectronic and excitonic properties of layered hybrid perovskites. *Phys. Rev. Mater.* 2: 1–12.

92 Passarelli, J.V., Fairfield, D.J., Sather, N.A. et al. (2018). Enhanced out-of-plane conductivity and photovoltaic performance in $n = 1$ layered perovskites through organic cation design. *J. Am. Chem. Soc.* 140: 7313–7323.

93 Kikuchi, K., Takeoka, Y., Rikukawa, M., and Sanui, K. (2005). Fabrication and characterization of organic-inorganic perovskite films containing fullerene derivatives. *Colloids Surfaces A Physicochem. Eng. Asp.* 257–258: 199–202.

94 Grancini, G., Roldán-Carmona, C., Zimmermann, I. et al. (2017). One-year stable perovskite solar cells by 2D/3D interface engineering. *Nat. Commun.* 8: 1–8.

95 Wang, Z., Lin, Q., Chmiel, F.P. et al. (2017). Efficient ambient-air-stable solar cells with 2D-3D heterostructured butylammonium-caesium-formamidinium lead halide perovskites. *Nat. Energy* 2: 1–10.

96 Poglitsch, A. and Weber, D. (1987). Dynamic disorder in methylammoniumtrihalogenoplumbates (II) observed by millimeter-wave spectroscopy. *J. Chem. Phys.* 87: 6373–6378.

97 Guo, Y., Yaffe, O., Paley, D.W. et al. (2017). Interplay between organic cations and inorganic framework and incommensurability in hybrid lead-halide perovskite $CH_3NH_3PbBr_3$. *Phys. Rev. Mater.* 1: 1–6.

98 Kieslich, G., Skelton, J.M., Armstrong, J. et al. (2018). Hydrogen bonding versus entropy: revealing the underlying thermodynamics of the hybrid organic-inorganic perovskite $[CH_3NH_3]PbBr_3$. *Chem. Mater.* 30: 8782–8788.

99 Pham, H.T., Duong, T., Rickard, W.D.A. et al. (2019). Understanding the chemical and structural properties of multiple-cation mixed halide perovskite. *J. Phys. Chem. C* 123: 26718–26726.

100 Hu, Y., Hutter, E.M., Rieder, P. et al. (2018). Understanding the role of cesium and rubidium additives in perovskite solar cells: trap states, charge transport, and recombination. *Adv. Energy Mater.* 8: 1–11.

101 Zhou, G. et al. (2018). Application of cesium on the restriction of precursor crystallization for highly reproducible perovskite solar cells exceeding 20% efficiency. *ACS Appl. Mater. Interfaces* 10: 9503–9513.

102 Habisreutinger, S.N. et al. (2014). Carbon nanotube/polymer composites as a highly stable hole collection layer in perovskite solar cells. *Nano Lett.* 14: 5561–5568.

103 Hou, Y., Zhou, Z.R., Wen, T.Y. et al. (2019). Enhanced moisture stability of metal halide perovskite solar cells based on sulfur-oleylamine surface modification. *Nanoscale Horizons* 4: 208–213.

104 Chaudhary, B., Kulkarni, A., Jena, A.K. et al. (2017). Poly(4-vinylpyridine)-based interfacial passivation to enhance voltage and moisture stability of lead halide perovskite solar cells. *ChemSusChem* 10: 2473–2479.

105 Cao, J., Yin, J., Yuan, S. et al. (2015). Thiols as interfacial modifiers to enhance the performance and stability of perovskite solar cells. *Nanoscale* 7: 9443–9447.

106 Abdelmageed, G., Sully, H.R., Bonabi Naghadeh, S. et al. (2018). Improved stability of organometal halide perovskite films and solar cells toward humidity via surface passivation with oleic acid. *ACS Appl. Energy Mater.* 1: 387–392.

107 Swarnkar, A., Chulliyil, R., Ravi, V.K. et al. (2015). Colloidal $CsPbBr_3$ perovskite nanocrystals: luminescence beyond traditional quantum dots. *Angew. Chem. Int. Ed.* 54: 15424–15428.

108 Wang, Y., Dar, M.I., Ono, L.K. et al. (2019). Thermodynamically stabilized β-$CsPbI_3$–based perovskite solar cells with efficiencies >18%. *Science (80-.)* 365: 591–595.

109 Hao, F., Stoumpos, C.C., Cao, D.H. et al. (2014). Lead-free solid-state organic-inorganic halide perovskite solar cells. *Nat. Photonics* 8: 489–494.

110 Li, X., Wu, Y., Zhang, S. et al. (2016). $CsPbX_3$ quantum dots for lighting and displays: roomerature synthesis, photoluminescence superiorities, underlying origins and white light-emitting diodes. *Adv. Funct. Mater.* 26: 2435–2445.

111 Boix, P.P., Nonomura, K., Mathews, N., and Mhaisalkar, S.G. (2014). Current progress and future perspectives for organic/inorganic perovskite solar cells. *Mater. Today* 17: 16–23.